Kinetic Studies of the Pt Carbonate-Mediated, Room-Temperature Oxidation of Carbon Monoxide by Oxygen over Pt/Al$_2$O$_3$ Using Combined, Time-Resolved XAFS, DRIFTS, and Mass Spectrometry

Mark A. Newton,*,[†] Davide Ferri,[‡] Grigory Smolentsev,[‡] Valentina Marchionni,[‡] and Maarten Nachtegaal[‡]

[†]Department of Physics, University of Warwick, Gibbet Hill Road, Coventry CV4 7AL, United Kingdom

[‡]Paul Scherrer Institut, CH-5232 Villigen, Switzerland

S *Supporting Information*

ABSTRACT: The kinetics involved in a recently revealed ambient-temperature mechanism for the catalytic oxidation of carbon monoxide by oxygen over a 5 wt % Pt/Al$_2$O$_3$ catalyst are evaluated within a periodic, plug flow, redox operation paradigm using combined mass spectrometry (MS), diffuse reflectance infrared spectroscopy (DRIFTS), and time-resolved Pt L$_3$-edge XAFS. The species that are the most active at room temperature are shown to be a high-wavenumber (ca. 1690 cm^{-1}) carbonate that we associate directly with a room-temperature redox process occurring in a fraction of the Pt atoms present in the catalyst. Our results, however, do not exclude the participation of carbonate species native to the Al$_2$O$_3$ support, though these species tend to store CO at ambient temperature and become significant participants in CO oxidation catalysis only at slightly higher temperatures (323−333 K). Pt carbonate formation (1690 cm^{-1}) under CO and the reaction to yield CO$_2$ is shown to be extremely rapid and subject to an average apparent activation energy (E^{app}), across the techniques applied, of 8.7 kJ mol^{-1}, within the temperature range investigated (276−343 K). Reoxidation of Pt (XANES) and subsequent CO$_2$ production mediated by Pt carbonates under O$_2$ (MS/IR) displays a first-order dependence upon O$_2$ partial pressure and a negative dependence upon the coverage of CO adsorbed on the Pt nanoparticles also present in this catalyst. This oxidative regeneration/CO$_2$ production step is subject to an apparent activation energy (E^{app}) of 56.5 (±5) kJ mol^{-1}, is kinetically limited by the desorption of molecular CO from Pt nanoparticles, and also is shown to be dependent upon the partial pressure of O$_2$ present in the oxidizing half of the cycle that we associate with the direct interaction of O$_2$ with molecular CO adsorbed on the nanoparticles that promotes their desorption. Finally, a minority reactive state producing CO$_2$ in the oxidizing cycle that displays no dependence upon the CO coverage of the nanoparticles can be induced through simple thermal treatment of the catalyst. These results are discussed in terms of the number and types of species present within the reactive system and in terms of the wider possibilities for the development of effective low-temperature CO oxidation using Pt/Al$_2$O$_3$ catalysts.
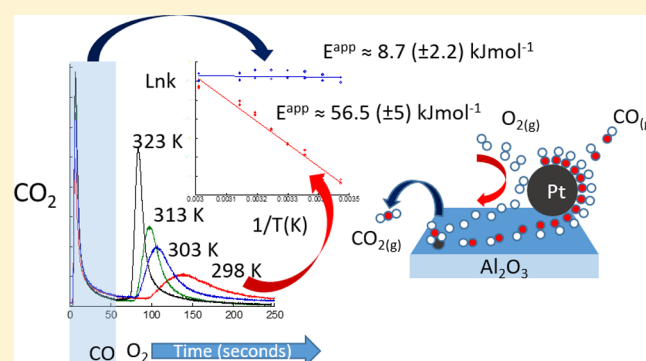
INTRODUCTION

Since Langmuir defined the Langmuir−Hinshelwood mechanism for the catalytic oxidation of carbon monoxide by O$_2$ over Pt wires,[1] the intervening decades have seen the catalytic oxidation of carbon monoxide by O$_2$ to yield CO$_2$ become the prototypical example of a heterogeneous, surface-mediated catalytic reaction.

As an industrially important catalytic process, CO oxidation by O$_2$ to yield CO$_2$ has few, if any, peers, and its global importance shows no sign of diminishing. Controlling emissions, particularly those arising from the use of internal combustion engines, as well as a variety of other clean air applications and the purification of feedstocks such as hydrogen all require that toxic CO be oxidized to CO$_2$.

However, the generally agreed upon Langmuir−Hinshelwood (LH) mechanism also fundamentally limits the applicability of Pt supported on nonreducible oxides at low temperatures. The LH mechanism requires that both molecular CO and dissociated oxygen be coadsorbed on the Pt nanoparticle surfaces for the oxidation of CO to be achieved. As a consequence, when the reaction temperature is decreased to below ca. 473 K, the competition for adsorption sites at Pt surfaces is progressively won by CO molecules. Eventually molecular CO covers the Pt, oxygen may no longer dissociate, and catalytic conversion is no longer possible.

Practically speaking, therefore, catalysts based purely upon Pt nanoparticles supported on nonreducible oxides such as Al_2O_3 are inactive below ca. 400 K. This apparently fundamentally limiting factor is highly problematic in many industrial arenas; in any real world application, one would like to minimize the amount of energy required to achieve sufficient activity, and there are many process situations where low-temperature activity is intrinsically required.

As a result, much research has been dedicated, with some deal of success, to deriving catalytic systems that are not subject to the limitations of the classic Langmuir−Hinshelwood mechanism as it manifests itself on Pt surfaces or supported Pt catalysts.

A number of catalytic systems, stemming from a time contemporary to Langmuir,[2,3] have been demonstrated to catalyze this conversion at much lower temperatures than simple Pt catalysts require. Research has shown that Co_3O_4,[4−7] supported Au nanoparticles,[8−10] and certain other combinations of noble metals with more exotic and reducible oxides (for instance, CeO_2,[11,12] Fe-based oxides,[13,14] $Pd/La/Al_2O_3$,[15] and Rh/TiO_2[16]) can achieve CO oxidation at low temperature. Equally, however, many of these highly active systems come with a variety of limitations and sensitivities, such as sintering of any supported nanoparticles and deleterious sensitivity to the presence of H_2O in the gas phase, a resistance to which may be required for practical operation. As such, by and large, platinum remains the metal of choice to achieve this conversion in many applied situations where the limitations imposed by the LH mechanism can be accepted.

Recent years have also seen some challenges to the fundamental details of the LH mechanism on Pt, such as the discovery of a number of highly reactive surface oxides and submonolayer O adlayers,[17−21] along with routes to O_2 dissociation actively assisted by adsorbed CO.[22] Although the surface oxides can be shown to be more reactive than metallic Pt surfaces, possibly to the point where they may catalyze CO oxidation at much lower temperatures, the existence of such phases does not, in and of itself, solve the problem of the poisoning of supported Pt by molecular CO adsorption.

Recently, Moses-DeBusk et al.[23] described a possible route to CO_2 that completely bypasses the requirement for metallic Pt nanoparticles. They derived a catalytic cycle that involves only isolated Pt atoms attached to the surface of θ-Al_2O_3 and proceeds via the formation and reaction of Pt carbonates formed at these atomically dispersed sites.

In complete contrast, Ding et al.[24] have also recently shown, using zeolitic (H-ZSM5) and Al-doped SiO_2 supports, that isolated Pt atoms present in these systems were only spectators of CO oxidation and water−gas shift catalysis at the relatively low temperature of 373 K. However, it is important to note that in their systems the exposure of isolated Pt atoms in their catalysts to CO resulted only in the formation of high-wavenumber (>2100 cm^{-1}) species in the infrared, which are indicative of the formation of linear CO species at these sites.

Following these studies, we demonstrated,[25] using a periodic redox approach to operation and a commercially available Pt/Al_2O_3 catalyst, that a Pt-carbonate mechanism over isolated Pt atoms located on the mixed θ/γ-Al_2O_3 support does exist and can be made catalytic at 298 K. These reactive carbonates are characterized by a broad infrared absorption between 1650 and 1700 cm^{-1}, whereas the high-wavenumber carbonyls characterized by Ding et al.[24] are not observed to be formed to any significant degree in our catalyst. The completion of the

catalytic cycle based upon these Pt carbonates[25] requires the active, but indirect, participation of the Pt nanoparticles that comprise the majority of the Pt in our catalyst. These Pt nanoparticles store molecular CO that can be transferred to the atomic Pt sites and be turned over to yield CO_2 during the oxidative phase of operation. We proposed that the reoxidation of the precursor sites to the $Pt(CO)_3$ species was also related to the removal of molecular CO from the Pt nanoparticles. Reoxidation of the precursors to the reactive carbonates was therefore dominated by an indirect pathway involving Pt nanoparticles rather than by a direct route as considered by Moses-DeBusk et al.[23]

In this article, we kinetically quantify the relationships that exist among the different Pt components found within this catalyst and show that the principal reactive species is a high-wavenumber carbonate that is not found to be readily observable on either the fresh T94 catalyst or indeed other unloaded aluminas (see below and the Supporting Information). We also show that Al_2O_3 carbonates may have a role to play in storing CO on the catalyst surface at ambient temperature and that they may decompose to any significant degree only at higher temperature.

Finally, we also address aspects of the catalyst pretreatment in an effort to understand how we might develop this novel mechanism to promote activity for CO oxidation toward a practical solution for the efficient removal of CO at ambient temperature using a relatively simple catalyst formulation based upon Pt.

■ EXPERIMENTAL SECTION

All operando experiments were carried out at the SuperXAS beamline of the Swiss Light Source (Villigen-PSI, Switzerland). Combined diffuse reflectance infrared Fourier transform spectroscopy and mass spectrometry (DRIFTS/MS) experiments were made using an offline laboratory attached to the SuperXAS beamline,[26] with a low-volume DRIFTS cell designed by Chiarello et al.[27] for transient experimentation. This was coupled to a Bruker Vertex 80 V infrared spectrometer fitted with a high-sensitivity MCT detector. The IR spectrometer was programmed to control the switching of fast solenoid valves (Parker) and to change between flows (50 mL min^{-1}) of Ar, CO/Ar (5 vol % or 0.4 vol % CO), O_2/Ar (2, 5, 10, or 20 vol % O_2), or 5 vol % H_2/Ar. For experimentation below ambient temperature, the cell was cooled prior to measurement using a flow of dry air passed via a Cu cooling coil immersed in a Dewar of liquid nitrogen. This permitted MS experimentation at temperatures to 276 K, though below ca. 283 K the IR was progressively affected by the condensation of H_2O onto the cell from the unpurged sample compartment.

The 5 wt % Pt/Al_2O_3 catalyst (25−35 mg, type 94, Johnson Matthey) was loaded into the DRIFTS cell and secured at either end using quartz wool. For DRIFTS/MS experiments, this cell was sealed on one side using a graphite disk and on the other side using a CaF_2 IR window. For XAFS/MS experimentation, this CaF_2 window was substituted by a Kapton window. The DRIFTS cell was heated using two cartridge heaters inserted on either side of the catalyst bed in the body of the cell; the sample temperature was measured using a 0.5 mm mineral-insulated type-K thermocouple inserted into the reactor inlet end of the catalyst bed and just in front of the region of the bed probed by the infrared or XAFS probes.

The loaded cell was then inserted into Harrick Praying Mantis infrared optics for DRIFTS experimentation and connected to the gas line for fast gas switching at the reactor inlet. The outlet was connected to a Pfeiffer MS via a stainless steel capillary maintained at a temperature of 423 K. The sample was thoroughly purged under Ar before being subjected to alternating flows of CO/Ar and O_2/Ar whose duration and number of repetitions were controlled by the infrared spectrometer. Alternatively, the sample would be pretreated
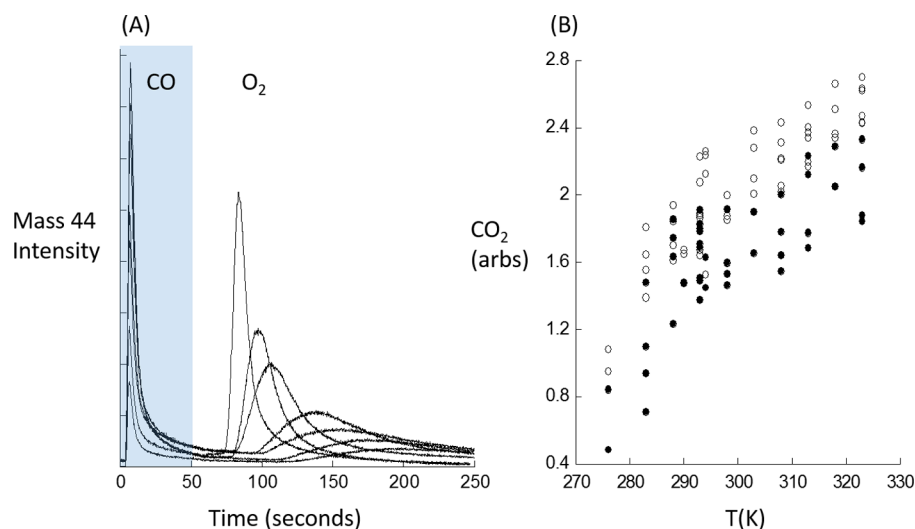
Figure 1. (A) Temperature dependence of CO_2 production observed during a single cycle of redox operation using 5 vol % CO/Ar and 21 vol % O_2/Ar feeds and for a previously untreated 5 wt % Pt/Al_2O_3 (type 94) catalyst. (B) Relative yield of CO_2 as a function of temperature observed in the MS for a number of cycles as a function of temperature: 5 vol % CO/Ar (solid circles); 21 vol % O_2/Ar (open circles). The switch to O_2 flow from CO occurs at 60 s.
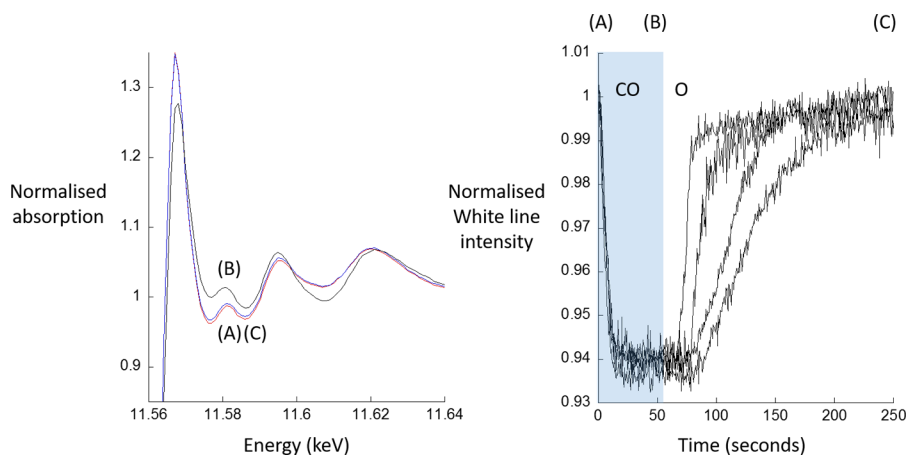

Figure 2. Normalized Pt L_3-edge XANES (left) and temporal variation in the normalized Pt L_3 white line intensity (right) during a single cycle of redox operation using 5 vol % CO/Ar and 21 vol % O_2/Ar feeds and in the temperature range of 298−333 K. The spectra in the left panel are taken from an experiment conducted at 298 K at the points [(A) red, (B) black, and (C) blue] indicated in the right-hand panel. In this case, the sample had been prereduced under flowing 5 vol % H_2/Ar to 573 K prior to cooling to RT and experimentation.

under O_2/Ar (TPO) or H_2/Ar (TPR) before being cooled and subjected to periodic CO/Ar:O_2/Ar operation.

During periodic operation, DRIFTS spectra were collected at 2 cm^{-1} resolution and with a time resolution of 0.433 s. MS data was collected for a number of pertinent masses while also recording the sample temperature and valve switching events, with a time resolution of <0.5 s per mass/signal.

For combined XAS/MS experimentation, the same overall protocols were used, though in this case the gas switching and experiment duration were controlled via hardware/software integrated into the SuperXAS beamline. Pt L_3-edge XAFS were recorded using a new fast monochromator based on an oscillating channel cut Si [111] monochromator operating at 2 Hz to yield four spectra per second.[26−28] EXAFS measurements were made in transmission using fast gridded ion chambers for the detection of the reference (I_o) and transmitted (I_t) X-rays. A third ionization chamber recorded a Pt foil reference for energy calibration.

EXAFS data were reduced using Prestopronto[29] or PAXAS[30] prior to analysis for structural information using EXCURV.[31]

RESULTS AND DISCUSSION

Kinetic Characterization of Carbonate-Mediated CO Oxidation under Reducing and Oxidizing Conditions. *Temperature Dependence of Low-T CO Oxidation.* Figure 1A depicts the temperature dependence of CO_2 production observed in MS for a single redox cycle of 5 vol % CO/ Ar:21 vol % O_2/Ar between 276 and 333 K and for a catalyst that has received no pretreatment, save for purging under Ar prior to use. This sample was then used to sequentially obtain the data shown. Figure 1B shows the relative yields of CO_2 for reducing and oxidizing halves of the cycles for a number of cycles at each temperature within this overall experiment.

The two halves of the catalytic chemistry can be seen to display rather distinct kinetic characters. Under oxidizing conditions, a clear temperature dependence is evident in terms of both the velocity and magnitude of the CO_2 production. The reaction with CO, however, shows only an enhanced yield with increasing temperature. In both cases, over
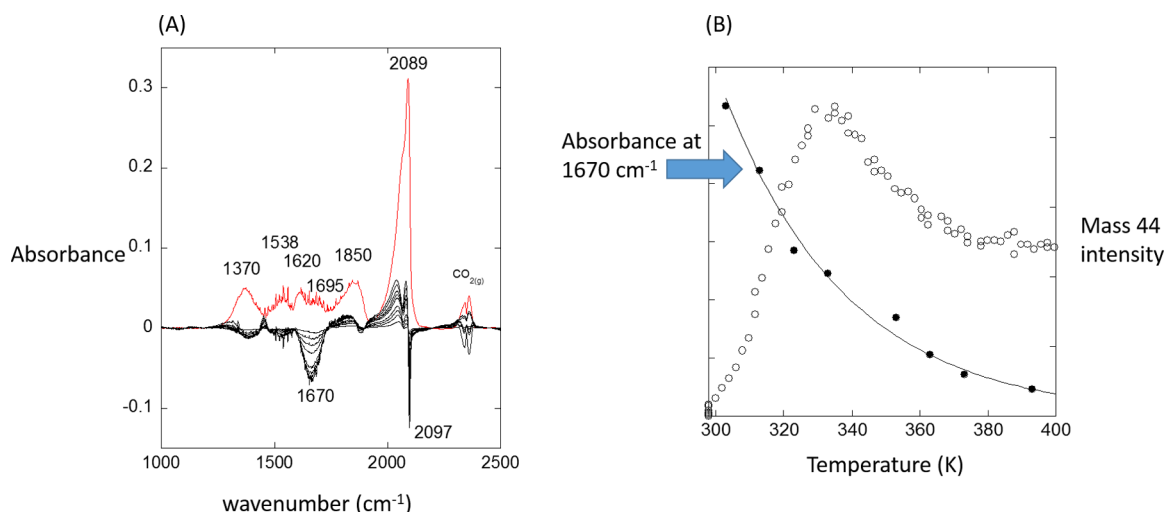
Figure 3. (A) Infrared spectrum (red) derived from an untreated sample exposed to a mixture of O_2 and CO in 4:1 ratio at RT and the evolution of this system as a function of temperature displayed via subsequent difference spectra (black). (B) Evolution of CO_2 as the sample is heated as compared to the change in intensity of the broad absorption centered at 1670 cm^{-1}.

the temperature range investigated, the CO_2 yield grows by a factor of 3 to 4 relative to that obtained at 276 K.

We also observe that the oxidizing part of the cycle always appears to produce slightly more CO_2 than the reaction under CO, and, though not explicitly evident from Figure 1, that the yield of CO_2 improves slightly over sequential cycles.

Figure 2 shows a similar set of experiments but viewed from the perspective of the Pt L_3 edge and specifically the intensity of the Pt L_3 white line that, to a first approximation, reflects changes in the oxidation state of the Pt in the temperature range of 298−333 K.

The view of this chemistry from the perspective of the Pt XANES well matches that of the MS. The magnitude of the changes in the XANES is small and, as we have previously demonstrated,[25] corresponds to (at most) only 10−20% of the Pt changing its oxidation state during this chemistry. Within this data there are some indications that there are small increases in the overall magnitudes of change with increasing temperature, but this is nowhere as clearly shown by this "point" probe than it is in the MS that is integrated over the entirety of the catalyst bed.

The spectra taken at points A and C are virtually identical and indicate that Pt has re-established its starting state by the end of the complete cycle. Spectrum B, collected just before reoxidation recommences, shows the maximal level of Pt reduction that has been achieved in the Pt phase.

Most notable, however, is the fact that the Pt L_3-edge XAS clearly evidence the reversible oxidation of a portion of the Pt at all. Oxidation of Pt surfaces and nanoparticles is not expected at ambient temperatures, and the simple chemisorption of oxygen, which might be expected in some parts of our experimental cycle, should not result in the changes we observe in the Pt L_3-edge white line. As such, on its own this observation is highly suggestive of a minority of the Pt existing in a non-nanoparticulate and possibly atomically dispersed state.

Figure 3A shows the results of heating a sample, previously exposed to a single CO/O_2 cycle at room temperature, at 10 K min^{-1}, under a 50 mL min^{-1} flow of O_2/CO in a 4:1 ratio from RT to 400 K and monitoring CO_2 production and changes in surface speciation. The red spectrum is that obtained at room temperature; black lines are difference spectra as the temper-

ature is increased. Figure 3B shows the corresponding evolution of CO_2 during this process along with its relation to the intensity of the broad band centered at 1670 cm^{-1} in the IR that changes most significantly in this temperature range. The room-temperature spectrum shows that exposure of this catalyst to a reaction mixture results in a significant variety of species. Those existing between ca. 1800 and 2100 cm^{-1} all relate to linear and bridging molecular CO adsorbed on Pt nanoparticles.[32] In the selected temperature range shown, these augment to varying degrees save for a high-wavenumber species at 2097 cm^{-1} that is progressively removed from the sample. This, alongside the corresponding growth of two lower-wavenumber IR bands, is suggestive of a rearrangement of the relative populations of molecularly adsorbed CO as the temperature increases: as we increase the temperature, some desorption of molecular CO commences and the adlayers rearrange as a result of the changing dipolar interactions between CO molecules that dominate their appearance in the IR at high coverages.[32] Below ca. 1800 cm^{-1}, the features observed in the starting spectrum may be associated with a variety of carbonate species on Al_2O_3 or Pt. The bands at ca. 1370 and 1538 cm^{-1} are assigned to monodentate carbonates adsorbed on the Al_2O_3.[33] These bands show some minor variations in intensity as the temperature is increased. Although this measurement does not rule them out as contributing elements to the reactive chemistry, the strong suggestion from IR is that they are not the predominantly active species. Bidentate carbonates and bicarbonate species on Al_2O_3 may show absorption bands in the 1640−1730 cm^{-1} region. However, such species always show prominent bands at ca. 1200−1300 cm^{-1}.[32] As such spectral features are not observed here, we can state that neither bidentate carbonates nor bicarbonates on the alumina support are playing any significant role in the observed chemistry. Therefore, it is only the broad difference feature centered at ca. 1670 cm^{-1} (in this difference plot) that is subject to significant removal as the temperature of the system is increased. The breadth of this band is such, however, that it may contain both species native to alumina (Supporting Information) and those associated with platinum carbonate within it. As such, though Figure 2B shows that the development of this band as species are removed correlates well
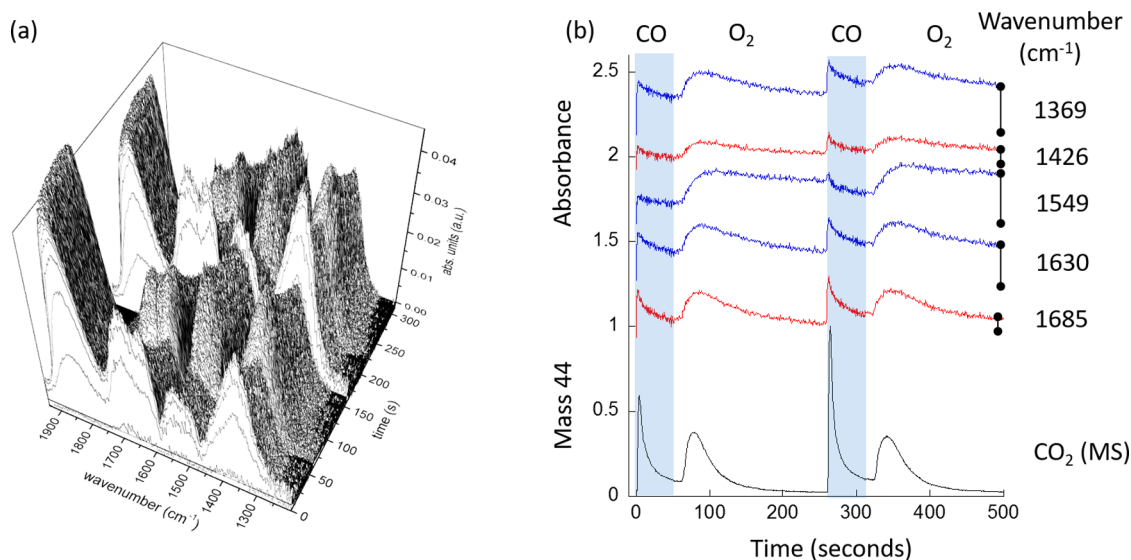
Figure 4. (a) Time-resolved DRIFTS spectra during two cycles of periodic redox operation (5 wt % CO/Ar followed by 20% O_2/Ar, 50 mL min^{-1}) at 298 K and for the 1940−1240 cm^{-1} region. (b) Temporal behavior of selected bands (as indicated) set against the corresponding evolution of CO_2 as observed during the cycling by MS.

with the CO_2 seen to be evolved, it cannot determine whether these are aluminum or platinum carbonates or, as seems most likely, both.

Indeed this correlation and the fact that a native reservoir or carbonates may be activated in this temperature range (Supporting Information) may well go some way to explain the increase in the yield of CO_2 as the reaction temperature is increased: either more sites are becoming available for reaction through each cycle and temperature or a greater fraction of the carbonates, whether they are hosted as Platinum or Aluminum Carbonates, react as the temperature is increased. We have shown that the CO_2 yield is a function of cycle number, at least in the initial stages of periodic operation.[25] However, Figure 3B would indicate that the peak in the CO_2 production at ca. 333 K is related to the inherent stability of these reactive carbonates (Supporting Information), convoluted with the background growth in CO_2 production. This background may arise either from some decomposition of the more thermally stable Al-carbonates or presage an increasing but yet still low-level contribution of conventional Pt LH catalysis as the adsorption/desorption equilibrium of molecular CO is probed by the increasing temperature. We had previously suggested that the feature at ca. 1690 cm^{-1} was the primary reactive species and was associated with reactive $Pt(CO_3)$ species.[25] However, the starting spectrum shown in Figure 3 along with the subsequent differences would indicate that more than a single $Pt(CO_3)$ species may be reacting to yield CO_2; indeed, the width of the absorption centered at 1670 cm^{-1} encompasses both the adsorbed $Pt(CO_3)$ species found by Moses-DeBusk et al.[23] (i.e., 1632 cm^{-1} on 0.18 wt % Pt/θ-Al_2O_3 and 1659 cm^{-1} on 1 wt % Pt/θ-Al_2O_3) or, as already mentioned, some carbonate species native to Al_2O_3.

That, at room temperature, the most active species present is a high-wavenumber carbonate (1690 cm^{-1}) whose behavior can be directly associated with the Pt redox events that have already been shown to be linked to the reactive chemistry (Figure 2) is shown in Figure 4.

Figure 4a shows time-resolved (0.4 s per spectrum) DRIFTS spectra during two CO/O_2 switching events at 298 K in the

1940−1240 cm^{-1} region to emphasize the behavior of the numerous species observed in this region and to allow them to be compared to the behavior of the molecular CO adsorbed on the Pt nanoparticles and as represented by the bridging CO band at ca. 1850 cm^{-1}. Figure 4b then details the behavior of each of the carbonate species in direct comparison to the evolution of CO_2 observed during the periodic operation.

What can be deduced from this figure is that all of the features due to carbonates of various types present on this catalyst have, to varying degrees, a relation to the evolution of CO_2. We associate the bands at 1369, 1549, and 1630 cm^{-1} with aluminum carbonate species (ref 33 and Supporting Information). In these cases, we can see that whereas they do show peaks of time-dependent concentration on the surface that correlate with CO_2 production, for the most part their levels only increase from cycle-to-cycle. As such, although they may be minority contributors to the reactive chemistry at room temperature, they mostly accumulate on the surface of the catalysts and act to store CO rather than convert it to CO_2 at this temperature.

The species responsible for the bands at 1426 and 1690 cm^{-1}, however, behave differently. Although they also have peaks and troughs in unison with the CO_2 production observed in MS, they return almost to the levels that they started from at each cycle. In other words, the species responsible for these features is reactive rather than passively accumulating. Moreover, the temporal behavior of these features can be seen to be in unison with the CO_2 production observed by MS and the redox behavior of the Pt observed in XAFS (Figure 2). The sum of the evidence therefore points to these being both the most active species at ambient temperature and associated with that proportion of the Pt actively engaged in changing the oxidation state at ambient temperature. We suggest that these two bands may arise from a single, bidentate Pt carbonate species of the type suggested by Moses-DeBusk et al.,[23] the symmetry/structure of which results in an intense asymmetric stretch at ca. 1689 cm^{-1}, with its less intense symmetric counterpart being found at 1425 cm^{-1}.
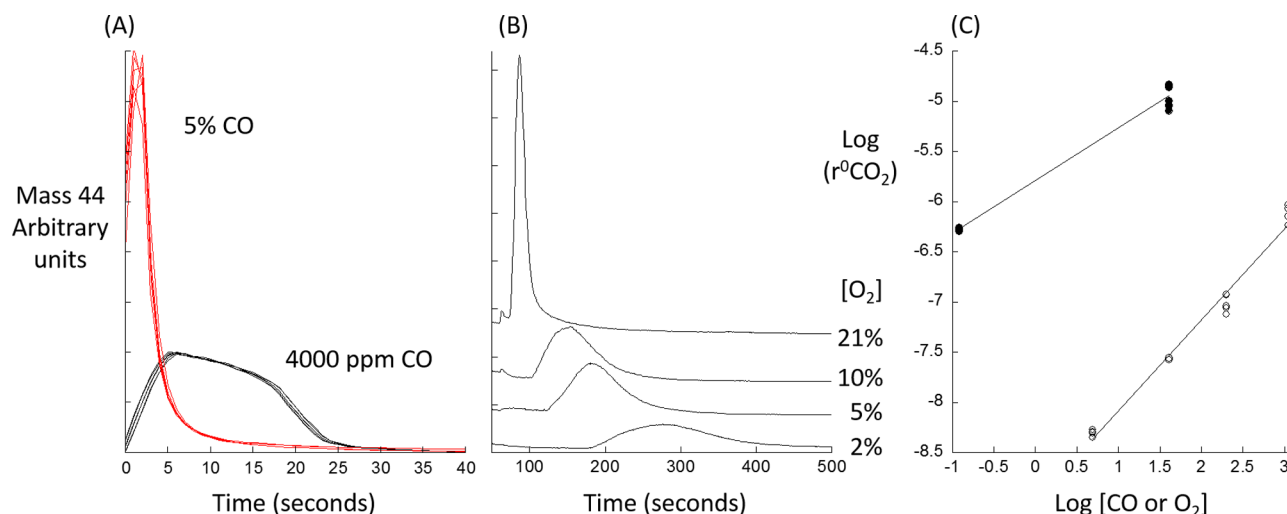
Figure 5. (A) Comparison of the mass 44 (CO_2) response during the reductive half of the operational cycle for 5 vol % CO/Ar (red) and 0.4 vol % CO/Ar (black) feeds. (B) Mass 44 (CO_2) evolution during the oxidative part of the cycle as a function of O_2 partial pressure as indicated. (C) Double log plots for each half of the cycle: solid circles (CO: 5 vol % CO and 0.4 vol % CO) and open circles (O_2: 2, 5, 10, 21 vol %). The switch between CO and O_2 flows occurs at $t = 60$ s.
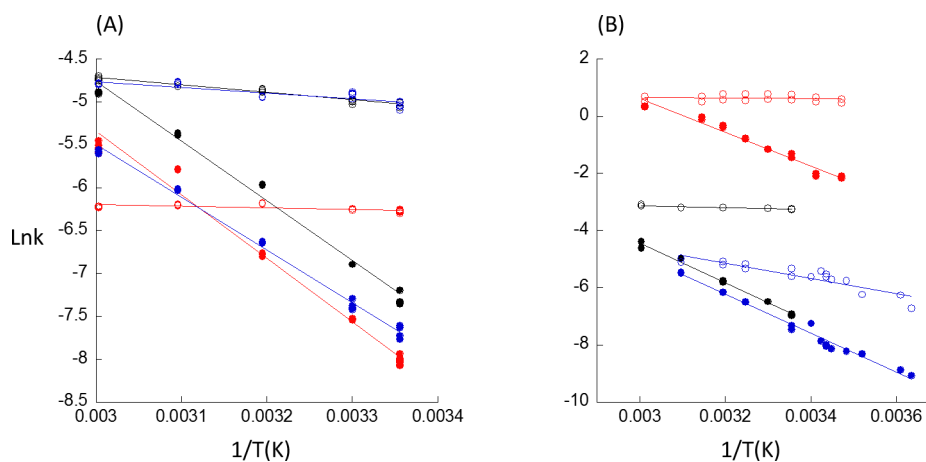

Figure 6. Arrhenius plots for CO_2 formation observed under CO (open symbols) and O_2 (filled symbols) within the periodic operation paradigm: (A) derived from MS; 0.4 vol % CO/5 vol % O_2 (red), 5 vol % CO/5 vol % O_2 (blue), 5 vol % CO/21 vol % O_2 (black); (B) for the 5 vol % CO/21 vol % O_2 case and derived from the carbonate band in DRIFTS (red), variation in the Pt L_3-edge white line intensity (black), and online MS (blue).

Apparent Orders of Reaction under CO- and O_2-Containing Feeds. Figure 5A shows the observed dependence of CO_2 production using feedstocks comprising 0.4 and 5 vol % CO diluted in Ar, and Figure 5B shows the equivalent data obtained by varying the oxygen concentration (2, 5, 10, and 21 vol % O_2 in Ar) at a constant reducing feed concentration of 5 vol % CO. All of these experiments were conducted at 298 K, and the data used was from online MS. Figure 5C shows a double log plot of the rate dependence in each case derived from the initial rates of CO_2 production derived from the MS traces.

Whereas CO_2 production under CO proceeds from the moment CO is introduced into the system (see also Figure 1A), induction times and the overall velocity of reaction are strong functions of the oxygen partial pressure in the oxidizing half of the reactive cycle. CO turnover, to form CO_2, in each half of the redox operation is dependent upon the concentration of the two reactants to varying degrees (Figure 3C). Under a CO feed, CO_2 production appears to be half order in CO concentration. Although this would perhaps be

consistent with the formation of the required carbonates involving a weakly bound CO precursor state with a finite lifetime and a diffusion-determined collection zone,[33−36] it is also possible that another dependence may lie hidden between the two extremes of CO concentration that we have been able to use. Once beyond the induction time observed in the oxidizing half of the reactive cycle (Figure 1), the net order of CO_2 production at 298 K appears to be close to unity with respect to O_2 concentration (Figure 5C). We also note the appearance, in the oxidizing side of the periodic operation, of a small CO_2 evolution that precedes the main reaction to yield CO_2 under O_2 and that occurs instantaneously with the switch from CO- to O_2-containing feeds. Minor though this state may be, it provides a clear indication that, in the oxidizing half of the cycle, a route to closing the catalytic cycle that is not subject to an induction time is possible. We will return to this observation later in the article.

Apparent Activation Energies of CO_2 Evolution in the Reducing and Oxidizing Halves of the Reactive Cycle. Figure 6 shows Arrhenius plots in the temperature range of 275−323

K derived from the three separate probes (MS, DRIFTS, and Pt L$_3$-edge XAFS). Table 1 summarizes the corresponding values

Table 1. Apparent Activation Energies (E^{app}) Derived for CO Oxidation for the Reducing and Oxidizing Halves of the Periodic Operation Employed to Study Low-Temperature CO Oxidation over 5 wt % Pt/Al$_2$O$_3$ Using Differing Pretreatments and Combinations of CO and O$_2$ Feeds, as Indicated[a]

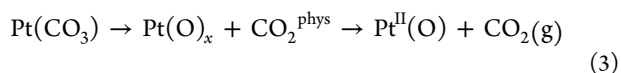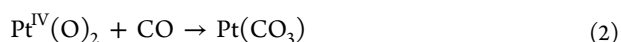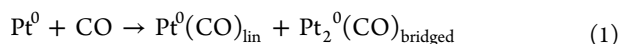| %O$_2$	%CO	pretreatment	probe	E^{app} (CO)	E^{app} (O$_2$)
21	5	573 K/H$_2$	MS	7.3	57.8
5	5	573 K/H$_2$	MS	5.5	51.0
5	0.4	573 K/H$_2$	MS	1.5	59.8
5	5	298 K/Ar	MS	13.7	54.5
5	5	523 K/O$_2$	MS	7.03	59.4
5	5	298 K/Ar	MS	16.6	59.3
5	21	473 K/O$_2$	MS	7.9	54.2
21	5	573 K/H2	Pt XANES	2.9	58.0
5	0.4	573 K/H$_2$	Pt XANES	2.3	54.8
5	21	523 K/O$_2$	DRIFTS	22.4	55.3
			mean	8.7	56.5
			std error	2.2	0.9

[a]The maximal temperature range investigated was 276−333 K. See also Figures 5 and 6.

of apparent activation energies (E_a^{app}) obtained from these analyses. As with the determination of the apparent orders of reaction, these plots have been made using the initial rates of change observed in CO$_2$ production (MS), the region of the IR spectrum associated with the Pt carbonate species (1800−1600 cm^{-1}), and the change in the white line intensity of the Pt L$_3$-edge in XAFS. We note that these methods sample the reacting system in differing ways. MS integrates over the entire volume of the catalyst bed, and DRIFTS and XAFS probe specific points (with differing volumes[37]) within it toward the reactor inlet.

First, these data show that from each probe we have applied, and irrespective of the manner in which they probe the catalyst bed, we obtain essentially the same results in terms of the overall kinetic character of the two CO oxidation pathways under investigation. As such, this would validate the sample environment[27] we have used to address this problem.

We also observe that differing pretreatments of the catalyst have precious little effect on the values obtained for E_{app} for either of the reactions under study.

Regarding the reaction occurring under the CO feed, we have recently postulated the following steps in the reaction to yield CO$_2$ at low temperature:[25]

$$Pt^0 + CO \rightarrow Pt^0(CO)_{lin} + Pt_2^0(CO)_{bridged} \quad (1)$$

$$Pt^{IV}(O)_2 + CO \rightarrow Pt(CO_3) \quad (2)$$

$$Pt(CO_3) \rightarrow Pt(O)_x + CO_2^{phys} \rightarrow Pt^{II}(O) + CO_2(g) \quad (3)$$

In these experiments, we are measuring a combination of steps 2 and 3: MS reports step 3, DRIFTS in the 1600−1700 cm^{-1} region addresses steps 2 and 3; and XAFS sees the system from the point of view of that fraction of Pt that is reacted from Pt^{IV} to a putative Pt^{II} oxidation state. From each perspective, CO$_2$ production during CO exposure is subject to virtually no apparent activation energy; it is only when the temperature is

lowered to below room temperature that we do see any indication of a measurable temperature dependence (Figure 6B, MS (blue)). This yields what we might regard as a maximal value for E^{app} of 22 kJ mol^{-1}, though the average value returned from these experiments and experimental viewpoints is substantially less (8.7 kJ mol^{-1}). As such, we may conclude that the available reactive Pt sites have an intrinsic ability to react with CO at around ambient temperature with a net barrier that is no more, and most likely less, than that previously derived for the remarkably reactive Co$_3$O$_4$ nanorods demonstrated by Xie and co-workers.[4] Equally, this result also appears at first sight to be at significant variance with the barrier (2.2204 eV/214 kJ mol^{-1}) to the decomposition of atomically dispersed O$_2$Pt^{IV}(CO$_3$) to yield CO$_2$ calculated from DFT by Moses-DeBusk et al.[23] However, these DFT calculations do not consider the prior accommodation of a physisorbed CO molecule at the Al$_2$O$_3$ surfaces studied in a precursor state or indeed the presence and possible effects of Pt nanoparticles existing near such centers. First, at room temperature, such a state may provide a locally enhanced reservoir of CO molecules that can seek out and react with the Pt atoms required to form a carbonate. Second, it may lead to geometrically different modes of interaction with these Pt sites that may be subject to much lower barriers than those derived by considering the direct interaction with gas-phase CO. Although we are not in a position to prove such hypotheses, we are able to note that this maximal value of E_a^{app} is virtually the same as the difference between the measured desorption energy of CO from α-Al$_2$O$_3$ and the postulated barrier to the surface diffusion of CO across that surface, with these parameters having been previously derived to successfully model CO oxidation over the model Pd/Al$_2$O$_3$ catalyst using the concept of a collection zone involving CO in a physisorbed precursor state.[35]

If we therefore assume that $E_a^{app} = E^{real} - E^{phys}$, where E^{real} is the actual net barrier to carbonate formation and reaction and E^{phys} is the heat of adsorption of CO into the physisorbed state (28 kJ mol^{-1}[35]), then we conclude that E^{real} can be no more ca. 50 kJ mol^{-1}. (Again, the mean value of E^{app} leads to a value of ca. 37 kJ mol^{-1}, Table 1). These values are now consistent with the energy difference (0.4356 eV/42 kJ mol^{-1}) calculated between an atomic and monodentate Pt(CO$_3$) species bound at an θ-Al$_2$O$_3$ surface and its decomposition products (CO$_2$(g)) and a partially reduced (Pt^{II}) center as calculated by Moses-DeBusk et al.[23]

As already shown above (Figures 1 and 4) and previously,[25] the major route to the reoxidation of the sites turned over in the reducing half of the cycle is subject to an induction time that we have shown above to be directly related to the oxygen concentration and the temperature. We have also postulated, on the basis of IR, that the same reservoir of CO that can react again with the reactive sites once they have been reoxidized also needs to be removed from the Pt nanoparticles present in this system before O$_2$ can be effectively supplied to the putative Pt^{II} sites that have been left after reaction with CO.

From the data shown above, the kinetic values of E^{app} detailed in Table 1 can be associated directly with the molecular desorption of CO. Moreover, we can apply the same analytical protocol to both the linear and bridging CO bands in the DRIFTS: this is shown in Figure 7 and shows that, in the oxidizing half of the cycle, the rate of reaction is controlled by the desorption kinetics of the CO adsorbed on the Pt nanoparticles that comprises the majority of the Pt in this system, quantitatively validating our original mechanistic
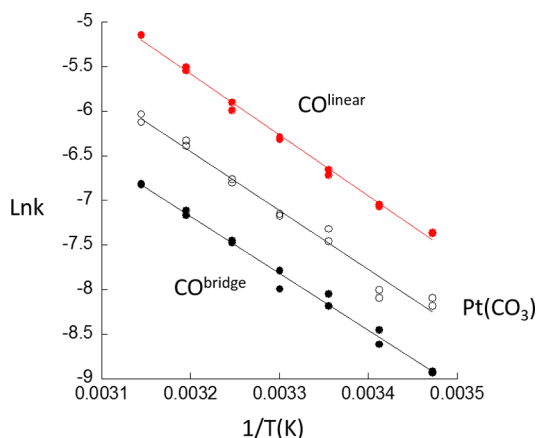
Figure 7. Arrhenius plots comparing the kinetic behavior of the bands associated with $Pt^{IV}(CO)_3$ with those derived from integrating over the spectral ranges corresponding to linear CO and bridged CO species adsorbed on the majority Pt^0 phase present within the catalyst. These plots are derived from experiments using 5 vol % CO/Ar and 21 vol % O_2/Ar.

proposal.[25] We note that this obtained value would have a magnitude (54–63 kJ mol^{-1}) reported by Allian et al.[21] for CO desorption from Al_2O_3-supported catalysts of a range of dispersions.

Equally, however, we point out that this value must be seen as corresponding to that for CO desorption from Pt nanoparticles and surfaces in the limit of high coverages of the type we undoubtedly have at certain stages of our experiments. The dependence of the heat of adsorption of CO on Pt surfaces is well established[38,39] to be a severe function of CO coverage and varying from ca. 180 kJ mol^{-1} in the limit of 0 coverage to 60 (Pt(110)[38] and 70 kJ mol^{-1} (Pt111)[39] as a result of the repulsive dipolar interaction occurring between the adsorbed CO molecules that also influence the coverage dependence of their IR spectra (Figure 3 and ref 32).

This conclusion, however, begs a further question as to what the results shown in Figure 5B might actually mean. If the reoxidizing cycle is controlled by the kinetics of desorption of molecular CO from the metallic nanoparticles in this system, then the apparent first-order dependence of the rate of CO_2 production on the oxygen concentration might be expected. However, what of the massive reduction in induction times in what are isothermal experiments carried out over the same catalyst?

This observation would imply that, in some way, increased levels of O_2 in the gas phase can promote CO desorption from Pt nanoparticles. We may, in this respect, only postulate as to how this may be occurring.

Allian et al.[21] found, from DFT calculations, evidence that direct interactions could occur between gas-phase O_2 and adsorbed CO molecules. These calculations assumed the formation of O−O*−C−O species that may provide a potential novel route toward CO_2 production. Indeed, prior to Allian et al.,[21] Ertl and co-workers[40] had also noted that CO domains and $O_{2(g)}$ could interact to cause complexity in the dissociative chemisorption of O_2 at low pressures over Pt(111).

Another possible explanation is that of collision-induced desorption, a phenomenon that has also been observed, and indeed used for analytical purposes, in other systems,[41] though it generally requires collision using hyperthermal gas-phase species.

Although we cannot be precise as to the origins of the behavior we observe with respect of the apparent promotion of CO desorption as a function of increasing O_2 partial pressure, as observed through a variable induction time for both CO desorption and subsequent CO turnover, we might reasonably conclude that this could be direct experimental evidence for O_2/CO interactions of the sort previously considered from a theoretical perspective.[21] However, in our case we do not arrive at the point where CO_2 production is the direct result of such interactions. Our results show only that molecular CO desorption is promoted, though this is indeed important as it reduces the induction time for the appearance of CO_2 in the oxidizing half of the cycle and therefore indirectly accelerates
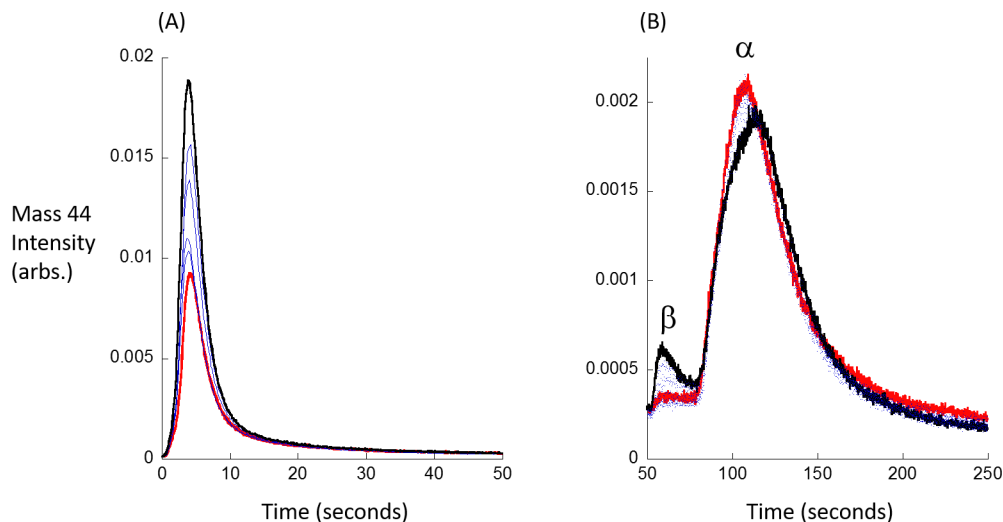

Figure 8. (A) CO_2 evolution as a function of pretreatment temperature during a redox cycle performed at 298 K: (A) under 5 vol % CO feed and (B) under 21 vol % O_2 feed. The red curves are obtained using no pretreatment save for flowing under Ar at RT prior to redox cycling at RT. The black curves shows the result obtained after heating the catalyst to 473 K under flowing Ar. The blue curves show the results obtained after heating to intermediate temperatures under Ar.
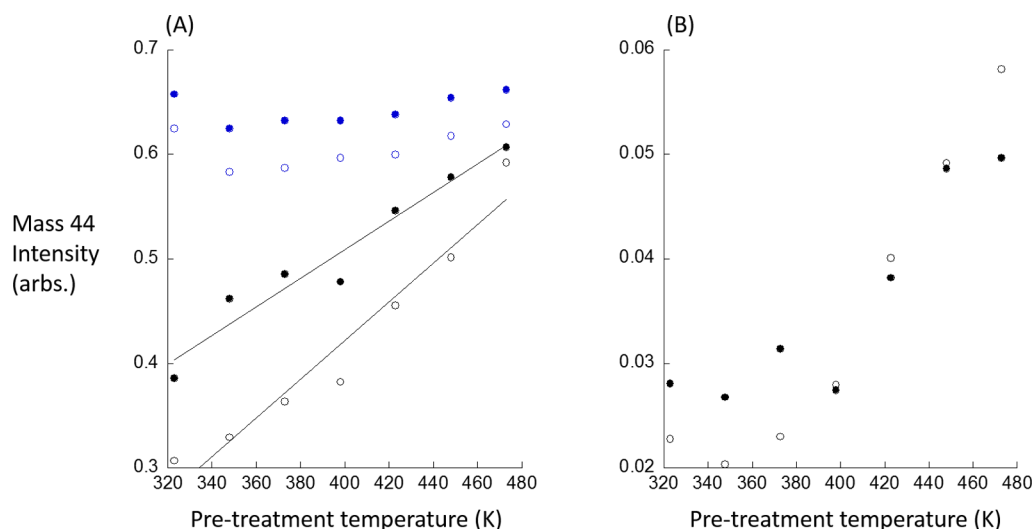
Figure 9. (A) Relative yields of CO_2 observed as a function of pretreatment temperature and for the first two redox cycles of CO: O_2 exposure at 298: black, under CO; blue, under O_2 for the α state; first cycle, open circles; second cycle, filled circles. (B) Relative yields for the β state occurring in the O_2 cycle: first cycle, open circles; second cycle, filled circles.

the closing of the catalytic cycle. That said, the very observation of an induction time is indicative of a state or reaction product that is formed through some form of intermediate that, under these circumstances, may well be weakly adsorbed molecular states of the type theoretically predicted by Allian and co-workers.[21]

Effects of Thermal Pretreatment of the Catalysts on the Character of Room-Temperature CO Oxidation. In our original report regarding this chemistry, we had used a sample that had been subjected to prior reduction in H_2 at 573 K; such a measurement showed that the species responsible for the low-temperature catalysis we had observed offered significant resistance to such a conventional reductive process. However, as is apparent from Figure 1 and Table 1, this catalyst can be used to affect the same chemistry in an as-received state with no prior pretreatment. Furthermore, we have also noticed that CO_2 yields from this chemistry increase with temperature up to ca. 333 K and that a minority reactive state in the oxidizing cycle can be seen to appear under certain circumstances. Hence, the effect of sequential thermal treatments of the system has also been studied. Figure 8 shows the results of this exercise, charting the velocities and yields of CO_2 obtained after heating the catalyst in Ar through a range of temperatures up to 473 K. Figure 9 quantifies the relative yields of CO_2 achieved at each temperature and for the three discrete CO_2-forming events observed.

These data confirm that simple heating of the catalyst, prior to reaction at room temperature, has two tangible effects on reactivity. First, in the CO half of the cycle a thermal pretreatment before use at 298 K can increase the yield of CO_2 by a factor of 2 in the first reactive cycle. Second, the simple thermal treatment can progressively induce what is labeled as the β state in Figure 8. This state is contrasted with that which we have labeled α in that it appears instantaneously with the switch from a CO- to an O_2-containing feed with no induction period associated with the production of CO_2. The CO_2 yield from this state increases by ca. a factor of 2.5 to 3 with thermal treatment to 473 K and eventually comprises ca. 10% of the total CO_2 produced in the oxidizing part of the cycle. The potential importance of the β state, with a view toward steady-state operation at RT, is clear: because it appears, and closes the

catalytic cycle, instantaneously and is therefore no longer subject to the kinetic limitations of CO desorption from the Pt nanoparticles imposed upon the α state, it offers the potential for significantly superior steady-state activity were it to be the major route present.

That these changes in reactivity can be induced by simple heating suggests two possibilities. The first is that adsorbed water and/or the level of hydroxylation at the surface of the alumina have roles to play in these events, blocking and otherwise interacting with potential reactive sites; the second is that by removing Al-carbonates through elevated temperature treatment new sites are created that may subsequently sequester Pt atoms, adding to the population of precursors to the Pt carbonates themselves. Experimental data and correlations of the intensity of the β state with the water and CO_2 evolved during the heating of both the T94 and an unloaded alumina sample are given as Supporting Information. These data show that both possibilities are occurring in the requisite temperature range and correlate to varying degrees with the appearance of the more reactive β state in the oxidizing part of the reaction cycle.

In this respect, Figure 8B (and also the Supporting Information) seems clear inasmuch as it indicates the former possibility, with the removal of water converting a proportion of α states to the more reactive β states (i.e., additional sites that might arise from the movement of Pt into sites previously occupied by water are not being created). Instead, dehydration and/or dehydroxylation modifies existing sites such that they behave in line with the mechanism due to Moses-DeBusk et al.[23] wherein reoxidation of the precursors to carbonate formation is direct, and there is no requirement for a separate metallic Pt phase to be present to affect a closing of the catalytic cycle.

How far this simply attained conversion of less reactive to instantaneously reactive sites in the oxidizing cycle of the experiment may be pushed and the precise nature of the sites involved, however, require further investigation.

What also appears to be clear, considering our results as compared to those recently published by Ding et al.,[24] is that not all isolated Pt atoms supported on Al-containing supports are the same: those that we have studied form[25] highly reactive

carbonates upon exposure to CO, whereas those elucidated by Ding et al.[24] form relatively stable linear carbonyls. As such, a much more comprehensive understanding of how and why these different isolated Pt species behave as they do, incorporating dependencies in the phase of Al_2O_3 present and what role hydration levels and degrees of hydroxylation might play, appears to be of considerable importance to the harnessing of what are, in the case of the carbonate forming species, potentially highly useful properties.

CONCLUSIONS

The ability of a commercially available 5 wt % Pt/Al_2O_3 to catalyze low-temperature CO oxidation under conditions of periodic operation has been characterized using combined MS, DRIFTS, and XAFS from structural and kinetic points of view. Our results validate a number of aspects of our recently proposed mechanism[25] to explain the behavior of this catalyst and have detailed temperature and feedstock dependencies. We have shown that, kinetically speaking, the formation and reaction of Pt carbonates associated with isolated Pt^{IV} sites in contact with the support are extremely facile, to a degree obtainable at temperatures of as low as 276 K and subject to minimal apparent energy barriers: at the very most, ca. 22 kJ mol^{-1}. At room temperature, therefore, the most active element in CO_2 production is a platinum carbonate characterized by high-wavenumber (1690 cm^{-1}) absorption in IR. Other carbonates native to the alumina may, by degrees, also participate in the production of CO_2, though at ambient temperature their primary function is to store CO that can be released again only at more elevated temperatures.

By contrast, the principal route to the regeneration of the sites active in carbonate formation and further CO turnover under O_2 is subject to both an induction period and an apparent activation energy of ca. 56.5 kJ mol^{-1}. This part of the catalytic cycle is demonstrably controlled by the desorption of CO from the majority metallic Pt component, yet the induction period can be reduced and the reaction velocity can be increased by increasing the partial pressure of O_2. The latter suggests that O_2 in the gas phase, or as a physisorbed entity, can promote the desorption of CO from the Pt nanoparticles to a significant degree and thereby accelerate reaction.

We have also shown that a more reactive minority state in the oxidizing part of the periodic operation can be induced through simple thermal treatments of the sample. This state does not suffer from an induction time, is subject to much reduced activation energies, and comprises evidence that a direct route to the reoxidation of isolated Pt sites may be attainable, in line with previous theoretical calculations.[23] The source of this reactive state is most likely dehydration, dehydroxylation, or removal at higher temperatures of the Al-carbonate functionality, which permits a more direct route to the reoxidation of the isolated Pt^{II} centers to exist. That such a reactive state can be formed indicates that ambient operation under steady-state conditions may be feasible if the precise reasons for its existence and how it may be optimized can be understood. Beyond this, it would appear that inducing a source of CO within a system that is subject to a lower barrier to CO desorption than from Al_2O_3-supported Pt nanoparticles but at the same time can mediate the delivery of oxygen to regenerate the sites required for carbonate formation is the key to further enhancing this chemistry toward practical and steady-state ends.

Finally, by contrasting our results with other recently published studies[24] it also seems clear that isolated Pt species formed on related Al-containing supports can display very different reactivities toward molecules such as CO. As such, a far more in-depth understanding of how and why such atomically disperse Pt centers show such different properties needs to be achieved so that those sites that form from relatively unreactive spectator species may be avoided and those that form, in the case of CO oxidation, highly reactive carbonates can be promoted. It seems likely that this will require an understanding of the structural difference between these atomically dispersed Pt states, how their formation relates to the phase of Al_2O_3 used (most likely on the basis of current evidence in the Boehmite-derived series γ, δ, and θ), and the degrees of hydration and hydroxylation present.

ASSOCIATED CONTENT

⑤ Supporting Information

The Supporting Information is available free of charge on the ACS Publications website at DOI: 10.1021/jacs.6b06819.

DRIFTS spectra, absorbance changes, and integrated levels of water (PDF)

AUTHOR INFORMATION

Corresponding Author
*E-mail: M.Newton.2@warwick.ac.uk

Notes
The authors declare no competing financial interest.

REFERENCES

(1) Langmuir, I. *Trans. Faraday Soc.* **1922**, *17*, 621.
(2) Merrill, D. R.; Scalione, C. C. *J. Am. Chem. Soc.* **1921**, *43*, 1982.
(3) Rogers, T. H.; Piggot, C. S.; Bahlke, W. H.; Jennings, J. M. *J. Am. Chem. Soc.* **1921**, *43*, 1973.
(4) Xie, X.; Liu, Z.-Q.; Haruta, M.; Shen, W. *Nature* **2009**, *458*, 746.
(5) Yao, Y. Y. *J. Catal.* **1974**, *33*, 108.
(6) Perti, D.; Kabel, R. L. *AIChE J.* **1985**, *31*, 1420.
(7) Thormählen, P.; Skoglundh, M.; Fridell, E.; Andersson, B. *J. Catal.* **1999**, *188*, 300.
(8) Haruta, M. *Catal. Today* **1997**, *36*, 153.
(9) Bond, G. C.; Thompson, D. T. *Catal. Rev.: Sci. Eng.* **1999**, *41*, 319.
(10) Hashmi, A. S. K.; Hutchings, G. J. *Angew. Chem., Int. Ed.* **2006**, *45*, 7896.
(11) Vayssilov, G. N.; Lykhach, Y.; Migani, A.; Staudt, T.; Petrova, G. P.; Tsud, N.; Skala, T.; Bruix, A.; Illas, F.; Prince, K. C.; Matolin, V.; Neyman, K. M.; Libuda, J. *Nat. Mater.* **2011**, *10*, 310.
(12) Carrettin, S.; Concepcion, P.; Corma, A.; Nieto, J. M. L.; Puntes, V. F. *Angew. Chem., Int. Ed.* **2004**, *43*, 2538.
(13) Qiao, B.; Wang, A.; Yang, X.; Allard, L. F.; Jiang, Z.; Cui, Y.; Liu, J.; Li, J.; Zhang, T. *Nat. Chem.* **2011**, *3*, 634.
(14) Chen, G. X.; Zhao, Y.; Fu, G.; Duschene, P. N.; Gu, L.; Zheng, Y. P.; Weng, X. F.; Chen, M. S.; Zhang, P.; Pao, C. W.; Lee, J. F.; Zheng, N. F. *Science* **2014**, *344*, 495.

(15) Peterson, E. J.; De La Riva, A. T.; Lin, S.; Johnson, R. S.; Guo, H.; Miller, H. T.; Kwak, J. H.; Peden, C. H. F.; Kiefer, B.; Allard, L. F.; Ribeiro, F. H.; Datye, A. K. *Nat. Commun.* **2014**, *S*, 4885.

(16) Guan, H.; Lin, J.; Qiao, B.; Yang, X.; Li, L.; Miao, S.; Liu, J.; Wang, A.; Wang, X.; Zhang, T. *Angew. Chem., Int. Ed.* **2016**, *55*, 2820.

(17) Ackermann, M. D.; Pedersen, T. M.; Hendriksen, B. L. M.; Robach, O.; Bobaru, S. C.; Popa, I.; Quiros, C.; Kim, H.; Hammer, B.; Ferrer, S.; Frenken, J. W. M. *Phys. Rev. Lett.* **2005**, *95*, 255505.

(18) Newton, M. A.; Chapman, K. W.; Thompsett, D.; Chupas, P. J. *J. Am. Chem. Soc.* **2012**, *134*, 5036.

(19) Butcher, D. R.; Grass, M. E.; Zeng, Z. H.; Askoy, F.; Bluhm, H.; Li, W. X.; Mun, B. S.; Somorjai, G. A.; Liu, Z. *J. Am. Chem. Soc.* **2011**, *133*, 20319.

(20) Miller, D.; Casalongue, H. S.; Bluhm, H.; Ogasawara, H.; Nilsson, A.; Kaya, S. *J. Am. Chem. Soc.* **2014**, *136*, 6340.

(21) Szlachetko, J.; Ferri, D.; Machionni, V.; Kambolis, A.; Safonova, O. V.; Milne, C. J.; Krocher, O.; Nachtegaal, M.; Sa, J. *J. Am. Chem. Soc.* **2013**, *135*, 19071.

(22) Allian, A. D.; Takanabe, K.; Fujdala, K. L.; Hao, X.; Truex, T. J.; Cai, J.; Buda, C.; Neurock, M.; Iglesia, E. *J. Am. Chem. Soc.* **2011**, *133*, 4498.

(23) Moses-DeBusk, M.; Yoon, M.; Allard, L. F.; Mullins, D. R.; Wu, Z. L.; Yang, X. F.; Veith, G.; Stocks, G. M.; Narula, C. K. *J. Am. Chem. Soc.* **2013**, *135*, 12634.

(24) Ding, K.; Gulec, A.; Johnson, A. M.; Schweitzer, N. M.; Stucky, G. D.; Marks, L. D.; Stair, P. C. *Science* **2015**, *350*, 189−192.

(25) Newton, M. A.; Ferri, D.; Smolentsev, G.; Marchionni, V.; Nachetegaal, M. *Nat. Commun.* **2015**, *6*, 8675.

(26) Frahm, R.; Nachtegaal, M.; Stotzel, J.; Harfouche, M.; van Bokhoven, J. A.; Grunwaldt, J. D. *AIP Conf. Proc.* **2010**, *1234*, 251.

(27) Chiarello, G. L.; Nachtegaal, M.; Marchionni, V.; Quaroni, L.; Ferri, D. *Rev. Sci. Instrum.* **2014**, *85*, 074102.

(28) Muller, O.; Lutzenkirchen-Hecht, D.; Frahm, R. *Rev. Sci. Instrum.* **2015**, *86*, 093905.

(29) Prestipino, C. *Software for Analysis of Quick Exafs and Dispersive XAFS Data*; https://code.google.com/p/prestopronto/.

(30) Binsted, N. *PAXAS: Programme for the Analysis of X-ray Adsorption Spectra*; University of Southampton, 1988.

(31) Binsted, N. *EXCURV98*, CCLRC Daresbury Laboratory computer programme, 1998.

(32) See, for instance, Hollins, P. *Surf. Sci. Rep.* **1992**, *16*, 51 and references therein..

(33) Busca, G.; Lorenzelli, V. *Mater. Chem.* **1982**, *7*, 89.

(34) Kisliuk, P. *J. Phys. Chem. Solids* **1957**, *3*, 95.

(35) Rumpf, T.; Poppa, H.; Boudart, M. *Langmuir* **1988**, *4*, 722.

(36) Bowker, M.; Bowker, L. J.; Bennett, R. A.; Stone, P.; Ramirez-Cuesta, A. *J. Mol. Catal. A: Chem.* **2000**, *163*, 221.

(37) See, for instance, Newton, M. A.; van Beek, W. *Chem. Soc. Rev.* **2010**, *39*, 4845.

(38) Wartnaby, C. E.; Stuck, A.; Yeo, Y. Y.; King, D. A. *J. Phys. Chem.* **1996**, *100*, 12483.

(39) Yeo, Y. Y.; Vattuonue, A.; King, D. A. *J. Chem. Phys.* **1997**, *106*, 392.

(40) Zambelli, T.; Barth, J. V.; Wintterlin, J.; Ertl, G. *Nature* **1997**, *390*, 495.

(41) See, for instance, Beckerle, J. D.; Johnson, A. D.; Ceyer, S. T. *Phys. Rev. Lett.* **1989**, *62*, 685; *J. Chem. Phys.* **1990**, *93*, 4047. Sonnenfroh, D. M.; Caledonia, G. E. *J. Geophys. Res.* **1993**, *98*, 21605. Szulczewski, G.; Levis, R. J. *J. Chem. Phys.* **1995**, *103*, 10238. Velic, D.; Levis, R. J. *J. Chem. Phys.* **1996**, *104*, 9629. Akerlund, C.; Zoric, I.; Kasemo, B. *Surf. Sci.* **1998**, *418*, 543. Asscher, M.; Zeiri, Y. *J. Phys. Chem. B* **2003**, *107*, 6903.